J|A|C|S
ARTICLES
Published on Web 02/14/2007

The Reactivity with CO of AHb1 and AHb2 from *Arabidopsis thaliana* is Controlled by the Distal HisE7 and Internal Hydrophobic Cavities

Stefano Bruno,[†] Serena Faggiano,[†] Francesca Spyrakis,[†] Andrea Mozzarelli,[†] Stefania Abbruzzetti,[‡] Elena Grandi,[‡] Cristiano Viappiani,*[,‡] Alessandro Feis,[§] Stephan Mackowiak,[§,||] Giulietta Smulevich,[§] Elena Cacciatori,[⊥] and Paola Dominici[⊥]

Contribution from the Dipartimento di Biochimica e Biologia Molecolare, Universitá degli Studi di Parma, Parma, Italy, Dipartimento di Fisica, Universitá degli Studi di Parma, Parma, Italy, Dipartimento di Chimica, Universitá degli Studi di Firenze; Sesto Fiorentino (FI), Italy, Dipartimento Scientifico e Tecnologico, Universitá degli Studi di Verona, Verona, Italy

Received September 17, 2006; E-mail: cristiano.viappiani@fis.unipr.it

Abstract: The nonsymbiotic hemoglobins, AHb1 and AHb2, have recently been isolated from *Arabidopsis thaliana*. Using steady-state and time-resolved spectroscopic methods, we show that Fe^{2+} AHb1 contains a mixture of penta- and hexacoordinated heme, while Fe^{2+} AHb2 is fully hexacoordinated. In the CO complexes, polar interactions and H-bonds with the ligand are stronger for AHb1 than for AHb2. The ligand binding kinetics are substantially different, reflecting the distribution between the penta- and hexacoordinated species, and indicate that protein dynamics and ligand migration pathways are very specific for each of the two proteins. In particular, a very small, non-exponential geminate rebinding observed in AHb1 suggests that the distal heme cavity is connected with the exterior by a relatively open channel. The large, temperature-dependent geminate rebinding observed for AHb2 implies a major role of protein dynamics in the ligand migration from the distal cavity to the solvent. The structures of AHb1 and AHb2, modeled on the basis of the homologous rice hemoglobin, exhibit a different cavity system that is fully compatible with the observed ligand binding kinetics. Overall, these kinetic and structural data are consistent with the putative NO-dioxygenase activity previously attributed to AHb1, whereas the role of AHb2 remains elusive.

Introduction

The genes for nonsymbiotic plant hemoglobins (Hbs) were first detected more than a decade ago.[1] Since then, several other plant hemoglobins have been isolated and heterologously expressed,[2,3] which are currently grouped into two classes characterized by different oxygen affinities, sequence similarities, and different expression patterns in response to environmental agents.[3,4] Class 1 hemoglobins are more closely related to the symbiotic leghemoglobins. A striking feature of nonsymbiotic Hb is hexacoordination of the heme iron through interactions with HisE7 and HisF8. Other hexacoordinated Hbs have recently been discovered. These include human neuroglobin (Ngb)[5] and cytoglobin,[6,7] as well as Hb from the sea cucumber *Caudina arenicola*.[8] As do the more common pentacoordinated Hbs, hexacoordinated Hbs in the Fe^{2+} state reversibly bind diatomic ligands such as O_2, CO, and NO with concomitant displacement of the endogenous ligand.

Two nonsymbiotic hemoglobins, termed AHb1 and AHb2 and belonging to class 1 and class 2, respectively, have been isolated from *Arabidopsis thaliana*[4] and have a sequence identity of approximately 60%. The expression of AHb1 is induced by low levels of oxygen[4] and exposure to nitrate[9] in both roots and rosette leaves. The latter response resembles the behavior of barley hemoglobin.[10] AHb1 has recently been suggested to be involved in NO detoxification by acting as an NO scavenger, thus reducing NO levels under hypoxic stress.[11] AHb2 is expressed at low levels in rosette leaves and is induced at low temperatures.[4] As the affinity for oxygen of AHb1 is extremely high ($K_d \approx 2-10$ nM),[4,12] it is unlikely that it functions as

[†] Dipartimento di Biochimica e Biologia Molecolare, Universitá degli Studi di Parma.
[‡] Dipartimento di Fisica, Universitá degli Studi di Parma.
[§] Dipartimento di Chimica, Universitá degli Studi di Firenze.
[⊥] Dipartimento Scientifico e Tecnologico, Universitá degli Studi di Verona.
[||] Present address: Department of Chemistry, Columbia University, New York, New York.

(1) Bogusz, D.; Appleby, C. A.; Landsmann, J.; Dennis, E. S.; Trinick, M. J.; Peacock, W. J. *Nature* **1988**, *331*, 178−180.
(2) Arredondo-Peter, R.; Hargrove, M. S.; Sarath, C.; Moran, J. F.; Lohrman, J.; Olson, J. S.; Klucas, R. V. *Plant Physiol.* **1997**, *115*, 1259−1266.
(3) Wang, Y. H.; Kochian, L. V.; Doyle, J. J.; Garvin, D. F. *Plant, Cell Environ.* **2003**, *26*, 673−680.
(4) Trevaskis, B.; Watts, R. A.; Andersson, C. R.; Llewellyn, D. J.; Hargrove, M. S.; Olson, J. S.; Dennis, E. S.; Peacock, W. J. *Proc. Natl. Acad. Sci. U.S.A.* **1997**, *94*, 12230−12234.
(5) Burmester, T.; Weich, B.; Reinhardt, S.; Hankeln, T. *Nature* **2000**, *407*, 520−523.
(6) Burmester, T.; Ebner, B.; Weich, B.; Hankeln, T. *Mol. Biol. Evol.* **2002**, *19*, 416−421.
(7) Trent, J. I.; Hargrove, M. S. *J. Biol. Chem.* **2002**, *277*, 19538−19545.
(8) Mitchell, D. T.; Ernst, S. R.; Hackert, M. L. *Acta. Crystallogr.* **1995**, *D51*, 760−766.
(9) Wang, R.; Guegler, K.; LaBrie, S. T.; Crawford, N. M. *Plant Cell* **2000**, *12*, 1491−1509.
(10) Nie, X.; Hill, R. D. *Plant Physiol.* **1997**, *114*, 835−840.
(11) Perazzolli, M.; Dominici, P.; Puertas, M. C. R.; Zago, E.; Zeier, J.; Sonoda, M.; Lamb, C.; Delledonne, M. *Plant Cell* **2004**, *16*, 2785−2794.

10.1021/ja066638d CCC: $37.00

an oxygen carrier. The affinity for oxygen of AHb2 is reportedly lower ($K_d \approx 140$ nM)[4,12] than that of AHb1.

The different oxygen binding properties and the induction by different external agents clearly suggest that there are distinct physiological functions for these two Hbs. In order to gain insights into structure−function relationships, we have characterized the heme moiety of AHb1 and AHb2 by resonance Raman (RR) and absorption spectroscopy and the binding of CO by rapid mixing and laser flash photolysis. These structural and kinetic characterizations revealed very different reactivities for the two proteins, likely arising from the presence of characteristic hydrophobic cavities and interactions of the ligand with distal cavity residues.

Materials and Methods

Cloning, Expression, and Purification of Recombinant AHb1 and AHb2. The cDNAs encoding AHb1 and AHb2 were inserted into pET11a (Novagen) and used to transform *Escherichia coli* BL21(DE3). The expression of the recombinant proteins was carried out in the presence of 30 μM hemin chloride at 24 °C. Recombinant AHb1 was purified by chromatography on a Q-Sepharose Fast Flow (GE Healthcare) column eluted with a 100 mM Tris buffer at pH 7.2. The protein was then loaded on a Q-Sepharose High Performance (GE Healthcare) column, and a linear gradient of NaCl from 0 to 0.1 M in 20 mM Tris buffer at pH 8.5 was used for elution. AHb2 was purified by chromatography using a Q-Sepharose High Performance column eluted with a linear gradient of NaCl from 0 to 0.2 M in 20 mM Tris buffer at pH 7.2. Approximately 8 mg of pure, ferrous oxygenated AHb1 and 15 mg of ferric AHb2 were obtained per liter of culture.

Sample Preparation. The deoxy AHb1 and AHb2 samples for stopped flow experiments were prepared by diluting the concentrated stock of the proteins with 100 mM sodium phosphate, 1 mM EDTA, pH 7.0 to a final concentration of 20−30 μM. The protein solution was mixed in the stopped-flow apparatus with the same buffer solution equilibrated with nitrogen/CO mixtures of known CO partial pressure. Sodium dithionite was added to a final concentration of 2 mM to both solutions. For flash photolysis experiments, both hemoglobins were diluted in 100 mM sodium phosphate buffer, 1 mM EDTA, pH 7.0 to a final concentration ranging from 60 to 70 μM. Before the experiment, solutions were equilibrated with nitrogen/CO mixtures of known CO partial pressure, and sodium dithionite was added to a final concentration of 2 mM.

The deoxy samples for resonance Raman (RR) spectroscopy were prepared by adding a fresh solution of sodium dithionite (Fluka Chemicals) to 30 μM protein solutions, which had been previously flushed with nitrogen. The final dithionite concentration was 20 mM. CO complexes for RR spectroscopy were prepared by first flushing the protein solutions with nitrogen, then flushing with ^{12}CO (Rivoira) or adding ^{13}CO (FluoroChem), and finally adding dithionite at 20 mM concentration. Protein concentrations ranged from 150 to 250 μM.

Resonance Raman. RR spectra were obtained at room temperature with excitation from the 413.1 nm line of a Kr^+ laser (Coherent). The back-scattered light from a slowly rotating NMR tube was collected and focused into a triple spectrometer (consisting of two Acton Research SpectraPro 2300i and a SpectraPro 2500i in the final stage with a 1800 or 3600 grooves/nm grating) working in the subtractive mode, equipped with a liquid nitrogen-cooled CCD detector (Roper Scientific Princeton Instruments). The spectra were calibrated to an accuracy of 1 cm^{-1} for intense isolated bands with indene, acetonitrile, and CCl_4 as standards.

Kinetic Studies. Stopped-flow experiments at a single wavelength were carried out using a temperature-controlled apparatus, manufactured by Applied Photophysics, using a 75-W xenon lamp as a light source and a photomultiplier as a detector. The instrumental dead time was 1.5 ms. CO binding kinetics were measured at 436 nm.

Scheme 1. Relevant Chemical Equilibria for the Reaction of CO with AHb1 and AHb2 (*Hb*) to Form the CO Complex (*HbCO*)[a]

$$\begin{array}{ccccc} & & (Hb_p :: CO) & & \\ & & k_c \uparrow\downarrow k_{-c} & & \\ HbCO & \underset{k_{-1}}{\overset{h\nu}{\rightleftharpoons}} & (Hb_p : CO) & \underset{k_{-2}}{\overset{k_2}{\rightleftharpoons}} & Hb_p + CO \\ & & k_{-a} \uparrow\downarrow k_a & & k_{-b} \uparrow\downarrow k_b \\ & & (Hb_h : CO) & \underset{k_{-3}}{\overset{k_3}{\rightleftharpoons}} & Hb_h + CO \end{array}$$

[a] Penta- and hexacoordinated species were indicated by the suffix *p* and *h*, respectively. ($Hb_{p,\,h}$: *CO*) indicates primary docking sites with CO still inside the distal pocket, while (Hb_p :: *CO*) indicates a site in which the photodissociated ligand is docked into an internal hydrophobic cavity, accessible from the primary docking site.

Flash photolysis was carried out with the circularly polarized second harmonic (532 nm) of a Q-switched Nd:YAG laser, and a CW Xe arc lamp as a probe source. The transient absorbance traces were measured at 436 nm through a 0.25-m spectrograph with a five-stage photomultiplier. The experimental setup was as described previously.[13,14] The cuvette had an optical path length of 2 mm. The repetition rate was about 0.3 Hz to allow for full sample recovery between laser flashes.

Typically 100 traces were averaged to yield a transient absorbance signal. Three time scales were used: 1 μs div^{-1}, 100 μs div^{-1}, 10 ms div^{-1}; 50,000 points were acquired for each trace. After preprocessing (baseline subtraction and pulse energy normalization) the transmitted intensity signal, $V(t)$, was converted to absorbance change, $\Delta A(t)$, with respect to the prepulse value (V_0) using the equation $\Delta A(t) = \log(V_0/V(t))$. The absorbance change signals, corresponding to the different time scales, were merged into a single curve covering several time decades. The time courses were subsequently logarithmically downsampled to give data sets of 300 points.

Kinetic Analysis of CO Rebinding Kinetics to AHb1 and AHb2. The minimal model necessary to account for the observed kinetics is sketched in Scheme 1 (vide infra). The differential equations associated with Scheme 1 were solved numerically, and the rate constants appearing in the equilibrium were optimized to obtain a best fit to the experimental data. Numerical solutions to the set of coupled differential equations corresponding to Scheme 1 were determined by using the function ODE15s within Matlab 7.0 (The MathWorks, Inc.). Fitting of the numerical solution to experimental data (and optimization of microscopic rate constants) was obtained with a Matlab version of the optimization package Minuit (CERN).

In order to improve the retrieval of microscopic rate constants, data from stopped flow and flash photolysis at the same temperature were simultaneously fitted, thus generating a set of rate constants at each temperature. This global analysis was repeated at several different temperatures between 10 °C and 40 °C. The advantage of the simultaneous fit arises from the specific sensitivity to different rate constants in laser flash photolysis (internal rates) and stopped flow (equilibrium between 5cHS and 6cLS species). The stability of the set of microscopic rate constants determined at each temperature was checked with global fits to rebinding kinetics at different CO concentrations. CO partial pressures ranged between 0.1 and 1 atm for flash photolysis experiments, and between 0.05 and 0.5 atm for stopped-flow experiments. The activation parameters for the microscopic rate constants were determined from the resulting linear Eyring plots (see Table 1).

Computational Modeling. The structures of AHb1 and AHb2 were modeled on the crystal structure of the homologous rice hemoglobin

(12) Watts, R. A.; Hunt, P. W.; Hvitved, A. N.; Hargrove, M. S.; Peacock, W. J.; Dennis, E. S. *Proc. Natl. Acad. Sci. U.S.A.* **2002**, *98*, 10119−10124.
(13) Abbruzzetti, S.; Sottini, S.; Viappiani, C.; Corrie, J. E. T. *J. Am. Chem. Soc.* **2005**, *127*, 9865−9874.
(14) Abbruzzetti, S.; Bruno, S.; Faggiano, S.; Grandi, E.; Mozzarelli, A.; Viappiani, C. *Photochem. Photobiol. Sci.* **2006**, *5*, 1109−1120.

Table 1. Microscopic Rate Constants from the Global Fit of the Stopped-Flow and Flash Photolysis Data at 20 °C

	AHb1			AHb2		
	k	$\Delta S^{\ddagger}$ (cal/mol K)	$\Delta H^{\ddagger}$ (kcal/mol)	k	$\Delta S^{\ddagger}$ (cal/mol K)	$\Delta H^{\ddagger}$ (kcal/mol)
k_{-1} (10^6 s^{-1})	5.13	–	–	22.2	–	–
k_2 (10^7 s^{-1})	9	-12.9 ± 0.6	2.7 ± 0.1	3.5	-4.4 ± 0.6	5.8 ± 0.2
k_{-2} (10^7 $M^{-1}s^{-1}$)	2.26	26 ± 2	14.7 ± 0.6	7.7	20.0 ± 0.8	12.4 ± 0.2
k_b (s^{-1})	23.5	12 ± 4	19 ± 1	334	-8 ± 2	11.7 ± 0.6
k_{-b} (s^{-1})	14.5	8 ± 4	18 ± 1	12	12 ± 4	19.2 ± 0.9
k_c (10^7 s^{-1})	2.07	–	–	–	–	–
k_{-c} (10^7 s^{-1})	0.25	–	–	–	–	–

[a] Activation enthalpies $\Delta H^{\ddagger}$ and entropies $\Delta S^{\ddagger}$ were estimated from the linear Eyring plots for each rate constant k_i in the temperature range 10–30 °C, according to the equation: $\ln(hk_i/k_BT) = \Delta S^{\ddagger}/R - \Delta H^{\ddagger}/RT$, where R is the gas constant, h is Planck's constant, and k_B is Boltzmann constant.

(PDB code 1d8u) using the program SwissPdbViewer. AHb1 and AHb2 show a 66% and a 54% identity with rice hemoglobin, respectively.

Tertiary structures for AHb1 and AHb2 were obtained by replacing the rice Hb1 primary sequence with the AHb1 or AHb2 amino acid residues using the MUTATE and CHARMM tools of SwissPdbViewer. The method was shown to be reliable in predicting the tertiary structure of other plant Hbs as soybean leghemoglobin.[15] The molecules were then read into Sybyl version 7.0 (www.tripos.com) and checked for proper atom and bond-type attributes. The hydrogens were added using the Biopolymer and Build/Edit menu tools and were energy minimized with the Powell algorithm and a gradient of 0.5 kcal (mol Å)$^{-1}$ for 1500 cycles, to remove potentially bad contacts. The analysis of cavity location and accessibility was performed by building Connolly surfaces of the whole proteins with Sybyl MOLCAD tools, using a sphere probe with a 1.4 Å radius.[16] The probe, rolling over the protein accessible areas, builds convex and concave surfaces, according to the presence of atoms well-exposed to the solvent or organized to form clefts and cavities. The topographical features of the protein surfaces were defined as a function of cavity depth. Hence, external protruding regions were colored blue, while cavities and clefts were colored green, yellow, and orange. The measurement of cavity depth was calculated by building, over the first molecular surface, a second surface with a 6.0 Å radius probe, unable to explore smaller cavities. The distance between these two generated surface maps is a direct measure of the cavity depth.[17] The AHb1 and AHb2 surfaces were also built progressively by decreasing the probe radius to the value of 1.0 Å to better investigate the accessibility of the potential CO binding sites and migration pathways. No substantial change of the surface profile, except an obvious expansion of all the cavities, was observed. Cavities were also directly analyzed with the program PASS, freely available on the web (http://www.ccl.net/cca/software/UNIX/pass/overview.shtml).[18] In order to include the presence of all the hydrogen atoms, the *hydrogen* option was adopted, thus using a default 1.5 Å radius probe, to investigate the accessibility of the internal tunnels. The area and the volume of the identified cavities were then estimated with the software Grasp (http://trantor.bioc.columbia.edu/grasp/).[19]

The hydrophobic character of the internal cavities was analyzed, in both AHb1 and AHb2 structures, using the molecular modeling software GRID, version 22a (www.moldiscovery.com),[20] using the xenon atom as the inquiring probe. Energetically and sterically favorable regions are identified by colored contours.

(15) Sáenz-Rivera, J.; Sarath, G.; Arredondo-Peter, R. *Plant Physiol. Biochem.* **2004**, *42*, 891–897.
(16) Sottini, S.; Abbruzzetti, S.; Spyrakis, F.; Bettati, S.; Ronda, L.; Mozzarelli, A.; Viappiani, C. *J. Am. Chem. Soc.* **2005**, *127*, 17427–17432.
(17) Keil, M.; Exner, T. E.; Brickmann, J. *J. Comput. Chem.* **2003**, *25*, 779–789.
(18) Binkowski, T. A.; Naghibzadeh, S.; Liang, J. *Nucleic Acids Res.* **2003**, *31*, 3352–3355.
(19) Nicholls, A.; Sharp, K.; Honig, B. *Proteins* **1991**, *11*, 281–296.
(20) Goodford, P. J. *J. Med. Chem.* **1985**, *28*, 849–857.

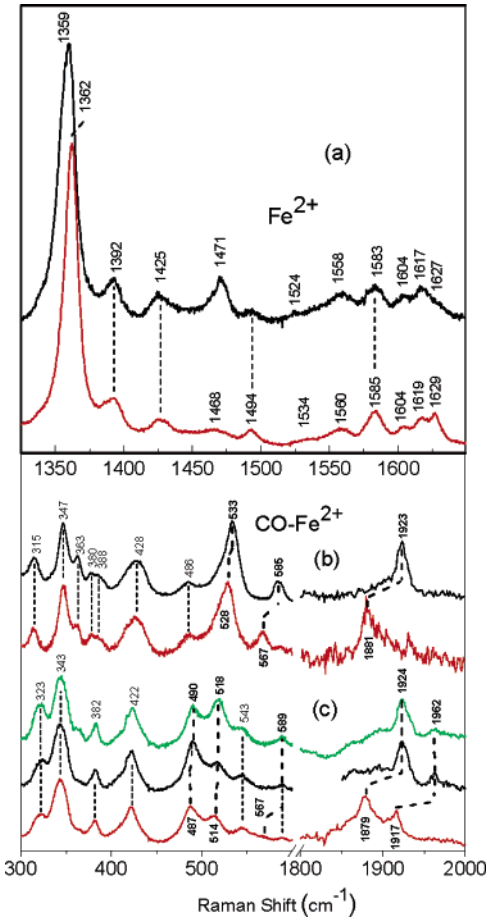

Figure 1. (a) RR spectra of Fe^{2+} AHb1 (black) and AHb2 (red). Laser power 20 mW (AHb1) or 10 mW (AHb2). (b) RR spectra of ^{12}CO (black) and ^{13}CO (red) complexes of Fe^{2+} AHb1 in 0.1 M Tris buffer, pH 8.1. Laser power 2 mW for ^{12}CO and 1 mW for ^{13}CO. (c) Resonance Raman spectra of the ^{12}CO (black) and ^{13}CO (red) complexes of Fe^{2+} AHb2 in 0.1 M phosphate buffer, pH 7.0, and of the ^{12}CO complex in 50 mM Tris buffer, pH 8.3 (green). Laser power was 2 mW.

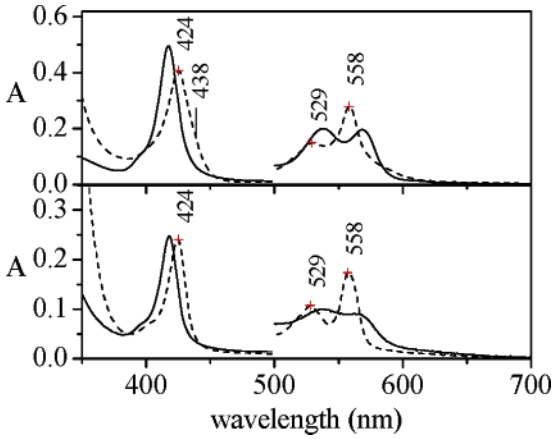

Figure 2. Absorption spectra of Fe^{2+} deoxy (dashed lines) and CO-bound (solid lines) AHb1 (27 μM) and Fe^{2+} AHb2 (14 μM). $T = 20$ °C.

Results and Discussion

Steady-State Spectroscopy. Resonance Raman (RR) (Figure 1, panel a) and electronic absorption spectra (Figure 2) of AHb1 and AHb2 in the Fe^{2+} state were indicative of the presence of hexacoordinated heme. However, in the case of AHb1, a substantial fraction of molecules displayed a pentacoordinated heme Fe. In addition to the typical spectrum of an Fe^{2+}

hexacoordinated low-spin (6cLS) complex with core-size marker bands at 1494 cm^{-1} (ν_3) and 1583 cm^{-1} (ν_2),[21] a ν_3 band at 1471 cm^{-1} (Figure 1a) indicates the existence of a pentacoordinated high-spin (5cHS) complex. This is also supported by the down shift of the ν_4 band from 1362 cm^{-1} in AHb2 to 1359 cm^{-1} in AHb1. UV−visible absorption spectra of AHb1 and AHb2 (Figure 2) further support these conclusions. The spectrum of Fe^{2+} AHb2 shows peaks at 424 nm (Soret band), 529 nm (β band), and 558 nm (α band), typically observed for 6cLS systems. The spectrum of Fe^{2+} AHb1 shows absorption maxima centered at the same wavelengths.[11] However, the presence of a less abundant 5cHS heme gives rise to a shoulder at 438 nm and broadens the spectrum between the α and β bands and at wavelengths longer than the α maximum. Using the absorbance spectra of Fe^{2+} deoxy AHb2 as a reference spectrum for a pure 6cLS species and that of Fe^{2+} deoxy human hemoglobin A as a reference for the pure 5cHS species, we could estimate that the fraction of 5cHS species in Fe^{2+} deoxy AHb1 is approximately 40%, with an equilibrium constant of 1.6. The observation of high-spin species in equilibrium with a 6cLS species has been previously reported for barley[22] and tomato[23] hemoglobins, which have a predominant 6cLS heme with a small amount of a 6cHS heme in the Fe^{3+} state, whereas a small 5c-HS component is observed in the Fe^{2+} state at neutral pH.

While the reaction of CO to Fe^{2+} AHb1 and AHb2 leads to formation of stable HbCO derivatives, exposure to oxygen causes rapid oxidation, especially for AHb2 (data not shown). The absorption spectra of CO−AHb1 and CO−AHb2 are shown in Figure 2. In the case of AHb1, the Soret peak is centered at 417 nm, and two peaks corresponding to the α and β bands are detectable at 569 and 538 nm, respectively. Similarly, for AHb2 the maximum of the Soret band is observed at 418 nm, whereas the α and β bands are at 562 and 538 nm.

We next investigated the RR spectra of the CO complexes of AHb1 and AHb2 to reveal the isotope-sensitive bands assignable to stretching and bending vibrations of the FeCO group. The ligand-related vibrational frequencies reflect the nature of the Fe−ligand bond and the ligand−protein interactions. In particular, polar interactions and the formation of H-bonds between the bound CO and the distal residues increase the extent of back-donation from the Fe d_π to the CO π^* orbitals. As a consequence, the Fe−C bond strengthens while the CO bond weakens, thereby increasing the ν(FeC) vibrational frequencies and decreasing the ν(CO) frequencies.[24−27] For a large class of CO adducts of heme proteins and model compounds containing an imidazole as the fifth ligand, a linear correlation between the frequencies of the ν(FeC) and ν(CO) stretching modes was found. The correlation plots have a negative slope and depend on the extent of π back-bonding. In the RR spectra of CO−AHb1 (Figure 1, panel b) the modes involving the CO ligand are ν(FeC) stretching at 533 cm^{-1} (528 cm^{-1} in ^{13}CO), δ(FeCO) bending at 585 cm^{-1} (567 cm^{-1} in ^{13}CO), and ν(CO) stretching at 1923 cm^{-1} (1881 cm^{-1} in ^{13}CO). The spectra are invariant in the pH range from 6 to 8, whereas a very weak band at 496 cm^{-1} appears at pH 5.5 (data not shown). The CO−AHb2 spectra display significant differences (Figure 1, panel c). At neutral pH, the prominent band at 490 cm^{-1} can be assigned to the ν(FeC) stretching on the basis of the 3 cm^{-1} isotopic shift in ^{13}CO. At pH 8.3, a new ν(FeC) stretching at 518 cm^{-1} (514 cm^{-1} in ^{13}CO) appears with a concomitant decrease of the band at 490 cm^{-1}. The other isotope-sensitive bands lie at 589 cm^{-1} [δ(FeCO)] (567 cm^{-1} in ^{13}CO), 1924 and 1962 cm^{-1} [ν(CO)] (1879, 1917 cm^{-1} in ^{13}CO). The RR spectra of the CO complexes of AHb1 and AHb2 suggest that polar interactions and H-bonds between the bound CO and the distal residues are very different for the two proteins.[24−27] The 496/490 cm^{-1} frequency of the ν(FeC) of AHb1/AHb2 together with the 1962 cm^{-1} frequency of the ν(CO) observed for AHb2 are typical of the complexes where CO is surrounded by a weakly polar environment.

Examples of such complexes are the CO adducts with porphyrins in solution, e.g., imidazole−protoporphyrin IX dimethyl ester,[28] and several CO−heme protein adducts at acidic pH, e.g., CO−myoglobin[29] and CO−horseradish peroxidase.[30] They are characterized by a low ν(FeC) frequency (491 cm^{-1} for myoglobin and 492 cm^{-1} for horseradish peroxidase) and a high ν(CO) frequency (1967 cm^{-1} for both cited proteins), owing to the reduced back-bonding extent. They are often loosely indicated as "open" forms, since the acid transition of myoglobin leads to a more open distal cavity,[31] although the aforementioned features—low ν(FeC) and high ν(CO)—are common both to proteins with an open distal cavity and to complexes with an apolar environment surrounding the bound CO molecule. In the present case, the slight *frequency* difference between 496 and 490 cm^{-1} is not significant, whereas the *intensity* difference is relevant. The fact that the "open" form predominates in the spectra of CO−AHb2 is a strong indication of reduced stabilizing interactions between the distal residues and the exogenous ligand. Moreover, the significant difference of the ν(FeC) frequency (533 cm^{-1} for AHb1 and 518 cm^{-1} for AHb2) indicates reduced back-donation degree and, therefore, stabilizing interactions weaker for the bound CO in AHb2 than for that in AHb1. This could be the consequence of a weaker H-bonding between the bound CO and the distal His in AHb2. This difference may be of functional significance, as it has been previously reported[32] that several mutated heme proteins [in which the distal cavity displays limited polarity (for example, the myoglobin H64L mutant)] have diminished O_2 affinity. Among these mutants, the distal His → Leu and His → Ala mutants have been studied by RR spectroscopy and are characterized by the typically low ν(FeC) frequencies of the

(21) Spiro, T. G.; Li, X. Y. In *Resonance Raman Spectra of Heme and Metalloproteins*; Spiro, T. G., Ed.; Biochemical Applications of Raman Spectroscopy, Vol. 3; John Wiley & Sons: New York, 1988; pp 1−37.
(22) Das, T. K.; Lee, H. C.; Duff, S. M. G.; Hill, R. D.; Peisach, J.; Rousseau, D. L.; Wittenberg, B. A.; Wittenberg, J. B. *J. Biol. Chem.* **1999**, *274*, 4207−4212.
(23) Ioanitescu, A. I.; Dewilde, S.; Kiger, L.; Marden, M. C.; Moens, L.; VanDoorslaer, S. *Biophys. J.* **2005**, *89*, 2628−2639.
(24) Spiro, T. G.; Wasbotten, I. H. *J. Raman Spectrosc.* **2005**, *34*, 725−736.
(25) Phillips, G. N. J.; Teodoro, M. L.; Smith, B.; Olson, J. S. *J. Phys. Chem. B* **1999**, *103*, 8817−8829.
(26) Ray, G. B.; Li, X. Y.; Ibers, J. A.; Sessler, J. L.; Spiro, T. G. *J. Am. Chem. Soc.* **1994**, *116*, 162−176.
(27) Li, T.; Quillin, M. L.; Phillips, G. N. J.; Olson, J. S. *Biochemistry* **1994**, *33*, 1433−1446.
(28) Evangelista-Kirkup, R.; Smulevich, G.; Spiro, T. G. *Biochemistry* **1986**, *25*, 4420−4425.
(29) Sage, J. T.; Morikis, D.; Champion, P. M. *Biochemistry* **1991**, *30*, 1227−1237.
(30) Smulevich, G.; Paoli, M.; DeSanctis, G.; Mantini, A. R.; Coletta, F. A. *Biochemistry* **1997**, *36*, 640−649.
(31) Morikis, D.; Champion, P. M.; Springer, B. A.; Sligar, S. G. *Biochemistry* **1989**, *28*, 4791−4800.
(32) Springer, B. A.; Sligar, S. G.; Olson, J. S.; Springer, G. N. J. *Chem. Rev.* **1994**, *94*, 699−714.

"open" CO-bound forms.[33] The reported lower O_2 affinity of AHb2 compared to that of AHb1[4,12] can therefore be correlated with the lower polarity of the active site.

It is likely that the main polar interaction between CO and the protein matrix involves H-bonding with the distal His. Thus, the observed differences in the spectra of the CO derivatives might be due to an indirect effect on the distal His repositioning when CO is bound rather than to a direct effect of amino acid replacement, since the amino acids which supposedly define the distal cavity in AHb1 do not have stronger H-bonding capabilities than those of AHb2, nor do they have an increased polarity. Upon CO binding, the distal His may rotate more freely in AHb2. It must be noted that even small changes in the amino acid sequence are sufficient to strongly change the interactions of CO with the distal cavity, as has been observed for recombinant cytochrome *c* peroxidase CCP(MI).[34,35] Recent work on a mutant form of type 1 nonsymbiotic hemoglobins from rice[36] also suggests an interaction between CO and the distal His, since the substitution of distal His with Leu causes the appearance of a ν(CO) band at relatively high wavenumbers (1958 cm^{-1}), which is typical of reduced polar interactions. Interestingly, several mutations at the B10 position, where a Phe residue is found in the native protein in close proximity to the distal His, also reduce the extent of polar interactions with the bound CO molecule.

Ligand Binding Kinetics. The coexistence of 5cHS and 6cLS species in deoxy Fe^{2+} AHb1, and purely 6cLS species in AHb2 (Figures 1 and 2), results in biphasic and monophasic stopped-flow CO binding kinetics to AHb1 and AHb2, respectively (see below). All phases appear to be thermally activated.

The CO rebinding kinetics following nanosecond laser photolysis of CO−AHb1 and CO−AHb2 solutions were recorded as a function of CO concentration (Figure 3a). The rebinding kinetics shown in Figure 3 report the fraction of deoxy hemes as a function of time after photolysis. The first data points correspond to the end of the laser pulse (~10 ns after the rise of the laser pulse signal, as detected by a fast PIN Si photodiode). The nanosecond photolysis yield measured for both Hbs, using human Hb A as a standard, is 1 within the experimental errors (10%, data not shown). Thus, data were scaled to 1 at the first data point. For AHb2 this may introduce a small systematic error, given the fast kinetic phase following photolysis, which may lead to partial rebinding of the photodissociated ligands before the end of the laser pulse. The short laser pulse width (5 ns fwhm) and the large bandwidth (500 MHz) of the detection system should minimize such artefacts. Picosecond time-resolved experiments will provide a better estimate of the fast kinetic phase.

The first striking feature of the rebinding curves is that, after photolysis of the CO−AHb1 complex, only a minor fraction of the photodissociated ligand reacts with the heme Fe on the nano- to microsecond time scale. By contrast, geminate rebinding accounts for about 30% of the photodissociated AHb2 molecules. The shape of the kinetics is independent of the photolysis level (data not shown), showing the absence of effects on the rate constants, due to conformational switching. The faster phase of the rebinding curves is essentially unaffected by the CO concentration, demonstrating that it reflects rebinding from within the protein matrix, whereas the bimolecular nature of the slower process is proved by the remarkable dependence on CO concentration. These experiments provide information on the different competitions of the internal ligand for the sixth coordination position in AHb1 and AHb2. While the slow phase of the ligand rebinding kinetics to AHb1 becomes slower and broader as the CO concentration is decreased, the progress curves for AHb2 demonstrate an increasing fraction of photodissociated molecules that remain in the deoxy state at 0.1 s. A similar dependence on CO concentration has been previously observed for other hexacoordinated hemoglobins such as neuroglobin[37−39] and tomato SOLly GLB1.[23] The slow rebinding fraction was attributed to photodissociated hemes, which have reacted with the endogenous competitor HisE7, and hence display much lower reactivity toward CO.

The temperature dependence of the rebinding kinetics (Figure 3b) revealed a very different response to thermal activation of the ligand migration processes inside the two proteins. Geminate rebinding in AHb1 was only marginally influenced by temperature, whereas a substantial increase in the amplitude of the

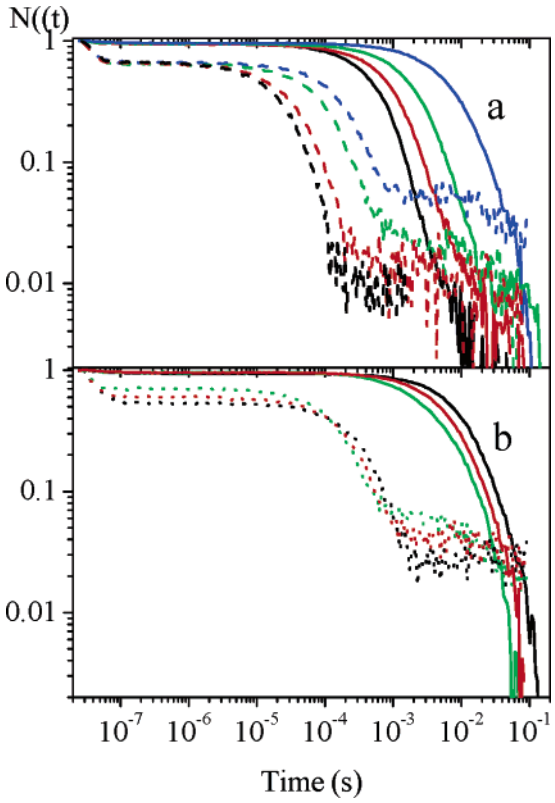

Figure 3. (a) CO rebinding kinetics to AHb1 (solid lines) and AHb2 (dotted lines), at 1 mM CO (black), 0.7 mM (red), 0.3 mM (green), and 0.1 mM (blue), at 25 °C. (b) CO rebinding kinetics to AHb1 (solid lines) and AHb2 (dotted lines), at 10 °C (black), 20 °C (red), and 30 °C (green). [CO] = 0.1 mM. Protein concentration was 60−70 μM.

(33) Anderton, C. L.; Hester, R. E.; Moore, J. N. *Biochim. Biophys. Acta.* **1997**, *1338*, 107−120.
(34) Wang, J.; Mauro, J. M.; Edwards, S. L.; Oatley, S. J.; Fishel, L. A.; Ashford, V. A.; Xuong, N. H.; Kraut, J. *Biochemistry* **1990**, *29*, 7160−7173.
(35) Smulevich, G.; Mauro, J. M.; Fishel, L. A.; English, A. M.; Kraut, J.; Spiro, T. G. *Biochemistry* **1988**, *27*, 5486−5492.
(36) Smagghe, B. J.; Sarath, G.; Ross, E.; Hilbert, J. L.; Hargrove, M. S. *Biochemistry* **2006**, *45*, 561−570.
(37) Kriegl, J. M.; Bhattacharyya, A. J.; Nienhaus, K.; Deng, P.; Minkow, O.; Nienhaus, G. U. *Proc. Natl. Acad. Sci. U.S.A.* **2002**, *99*, 7992−7997.
(38) Uzan, J.; Dewilde, S.; Burmester, T.; Hankeln, T.; Moens, L.; Hamdane, D.; Marden, M. C.; Kiger, L. *Biophys. J.* **2004**, *87*, 1196−1204.
(39) Kiger, L.; Uzan, J.; Dewilde, S.; Burmester, T.; Hankeln, T.; Moens, L.; Hamdane, D.; Baudin-Creuza, V.; Marden, M. C. *IUBMB Life* **2004**, *56*, 709−719.

geminate phase was observed for AHb2, when the temperature was decreased. This finding indicates that the photodissociated ligand can easily escape from the distal pocket of AHb1 to the solvent, with little assistance from protein dynamics. At variance, in the case of AHb2, thermal activation had noteworthy effects on the rebinding rate. This clearly pointed to a substantial role of protein fluctuations in regulating the exchange of the ligand between the distal pocket and the solvent. In addition, as the temperature increases, a larger fraction of slow phase is observed, indicating a higher activation energy for binding of the internal (His) ligand relative to that for the binding of a diatomic ligand.[38]

In defining a minimal model capable of accounting for the observed kinetics, we made use of the accumulated knowledge on the much more studied myoglobin and human hemoglobin A. It is well accepted that protein dynamics are essential in modulating the function of heme proteins, as demonstrated for human hemoglobin A[40−42] and myoglobin[43−47] by kinetic investigations under a variety of experimental conditions. In particular, the analysis of rebinding kinetics upon flash photolysis of CO complexes as a function of temperature and viscosity has allowed for the detection of structural relaxations triggered by the photolysis of the ligand, leading to nonexponential geminate rebinding kinetics.[44,48−50]

More recently, the hydrophobic cavities to which the photodissociated ligands transiently bind were shown to play an essential role in the function of several heme proteins, as they allow for simultaneous binding of substrates and confinement of unstable reaction intermediates. For myoglobin, it has been directly demonstrated that dissociated ligands can access internal cavities, or packing defects, referred to as xenon cavities.[51,52] The kinetic phases received a new interpretation as cryogenic and time-resolved X-ray crystallography led to the identification of well-defined ligand binding sites within the protein matrix.[52−57] Only in the case of myoglobin was the interplay between ligand binding, migration, and structural relaxation unequivocally demonstrated to influence ligand binding kinetics both from experimental and theoretical points of view.[47,58−60]

The typical kinetic signatures associated with ligand migration upon laser flash photolysis of CO complexes have been recognized for several heme proteins including truncated hemoglobins[61] and human hemoglobin A, both in the R[16,62] and the T states,[63] in addition to myoglobin.

Attempts to fit the geminate recombination to AHb1 with a stretched exponential decay did not give good results, while the data could be perfectly reproduced with a double exponential decay (not shown). This suggests that protein relaxation has little influence on this kinetic phase while it hints to the possible involvement of a secondary docking site modulating its kinetics.

The minimal model we have chosen to account for the observed kinetics is shown in Scheme 1 and, in addition to ligand migration, requires competitive binding between the exogenous (CO) and the endogenous (HisE7) ligands.[23,37−39,64−66] The differential equations associated with Scheme 1 were solved numerically, and the microscopic rate constants were obtained by a simultaneous fit to stopped-flow and flash photolysis data at the same temperature. This global analysis was then repeated at several CO concentrations. The advantage of the simultaneous fit arises from the specific sensitivity to different rate constants in laser flash photolysis (internal rates) and stopped flow (equilibrium between 5cHS and 6cLS species).

Similarly to what was done for myoglobin and hemoglobin,[16,47,67,68] distinct geminate states are explicitly included in Scheme 1, where (Hb_p::CO) represents a secondary docking site, accessible from the primary site in the distal pocket. We neglected relaxation of (Hb_p::CO) to (Hb_h::CO) as the lifetime of CO in this trap is much shorter than the time it takes for HisE7 to bind the heme Fe (vide infra).

CO escapes from AHb2 with a fast, thermally activated, single-exponential process in the investigated temperature range with an apparent lifetime of 14 ns at 20 °C, suggesting that neither structural relaxation nor ligand migration to multiple docking sites significantly affects ligand rebinding on this time scale. The equilibrium between 5cHS and 6cLS species influences only the slower portion of the flash photolysis kinetics, while it affects the overall time course of the stopped-flow data.

The escape of CO from the protein matrix is much easier in the case of AHb1, as demonstrated by the small amplitude of the geminate phase. However, geminate rebinding is nonexponential, reflecting at least two kinetic phases, which were

(40) Eaton, W. A.; Henry, E. R.; Hofrichter, J.; Mozzarelli, A. *Nat. Struct. Biol.* **1999**, *6*, 351−358.
(41) Henry, E. R.; Jones, C. M.; Hofrichter, J.; Eaton, W. A. *Biochemistry* **1997**, *36*, 6511−6528.
(42) Viappiani, C.; Bettati, S.; Bruno, S.; Ronda, L.; Abbruzzetti, S.; Mozzarelli, A.; Eaton, A. W. *Proc. Natl. Acad. Sci. U.S.A.* **2004**, *101*, 14414−14419.
(43) Austin, R. H.; Beeson, K. W.; Eisenstein, L.; Frauenfelder, H.; Gunsalus, I. C. *Biochemistry* **1975**, *14*, 5355−5373.
(44) Ansari, A.; Jones, C. M.; Henry, E. R.; Hofrichter, J.; Eaton, W. *Biochemistry* **1994**, *33*, 5128−5145.
(45) Kleinert, T.; Doster, W.; Leyser, H.; Petry, W.; Schwarz, V.; Settles, M. *Biochemistry* **1998**, *37*, 717−733.
(46) Librizzi, F.; Viappiani, C.; Abbruzzetti, S.; Cordone, L. *J. Chem. Phys.* **2002**, *116*, 1193−1200.
(47) Dantsker, D.; Samuni, U.; Friedman, J. M.; Agmon, N. *Biochim. Biophys. Acta.* **2005**, *1749*, 234−251.
(48) Steinbach, P. J. *Biochemistry* **1991**, *30*, 3988−4001.
(49) Tian, W. D.; Sage, J. T.; Srajer, V.; Champion, P. M. *Phys. Rev. Lett.* **1992**, *68*, 408−411.
(50) Lim, M.; Jackson, T. A.; Anfinrud, P. A. *Proc. Natl. Acad. Sci. U.S.A.* **1993**, *90*, 5801−5804.
(51) Tilton, R. F. J.; Kuntz, I. D. J.; Petsko, G. A. *Biochemistry* **1984**, *23*, 2849−2857.
(52) Ostermann, A.; Washipky, R.; Parak, F. G.; Nienhaus, G. U. *Nature* **2000**, *404*, 205−208.
(53) Schlichting, I.; Berendzen, J.; Phillips, G. N.; Sweet, R. M. *Nature* **1994**, *371*, 808−812.
(54) Srajer, V.; Ren, Z.; Teng, T. Y.; Schmidt, M.; Ursby, T.; Bourgeois, D.; Pradervand, C.; Schildkamp, W.; Wulff, M.; Moffat, K. *Biochemistry* **2001**, *40*, 13802−13815.
(55) Vojtechovsky, J.; Chu, K.; Berendzen, J.; Sweet, R. M.; Schlichting, I. *Biophys. J.* **1999**, *77*, 2153−2174.
(56) Schotte, F.; Lim, M.; Jackson, T. A.; Smirnov, A. V.; Soman, J.; Olson, J. S.; Phillips, G. N., Jr.; Wulff, M.; Anfinrud, P. A. *Science* **2003**, *300*, 1944−1947.
(57) Bourgeois, D.; Vallone, B.; Schotte, F.; Arcovito, A.; Miele, A. E.; Sciara, G.; Wulff, M.; Anfinrud, P.; Brunori, M. *Proc. Natl. Acad. Sci. U.S.A.* **2003**, *100*, 8704−8709.
(58) Agmon, N. *Biophys. J.* **2004**, *87*, 1537−1543.
(59) Schmidt, M.; Nienhaus, K.; Pahl, R.; Krasselt, A.; Anderson, S.; Parak, F.; Nienhaus, G. U.; Srajer, V. *Proc. Natl. Acad. Sci. U.S.A.* **2005**, *102*, 11704−11709.
(60) Bourgeois, D.; Vallone, B.; Arcovito, A.; Sciara, G.; Schotte, F.; Anfinrud, P. A.; Brunori, M. *Proc. Natl. Acad. Sci. U.S.A.* **2006**, *103*, 4924−4929.
(61) Samuni, U.; Dantsker, D.; Ray, A.; Wittenberg, J. B.; Wittenberg, B. A.; Dewilde, S.; Moens, L.; Ouellet, Y.; Guertin, M.; Friedman, J. M. *J. Biol. Chem.* **2003**, *278*, 27241−27250.
(62) Sottini, S.; Abbruzzetti, S.; Viappiani, C.; Bettati, S.; Ronda, L.; Mozzarelli, A. *J. Phys. Chem. B* **2005**, *109*, 11411−11413.
(63) Samuni, U.; Roche, C. J.; Dantsker, D.; Juszczak, L. J.; Friedman, J. M. *Biochemistry* **2006**, *45*, 2820−2835.
(64) Hargrove, M. S. *Biophys. J.* **2000**, *79*, 2733−2738.
(65) Trent, J. T. I.; Hvitved, A. N.; Hargrove, M. S. *Biochemistry* **2001**, *40*, 6155−6163.
(66) VanDoorslaer, S.; Dewilde, S.; Kiger, L.; Nistor, S. V.; Goovaerts, E.; Marden, M. C.; Moens, L. *J. Biol. Chem.* **2003**, *278*, 4919−4925.
(67) Sottini, S.; Abbruzzetti, S.; Viappiani, C.; Ronda, L.; Mozzarelli, A. *J. Phys. Chem. B* **2005**, *109*, 19523-19528.
(68) Abbruzzetti, S.; Giuffrida, S.; Sottini, S.; Viappiani, C.; Cordone, L. *Cell Biochem. Biophys.* **2005**, *43*, 431−438.

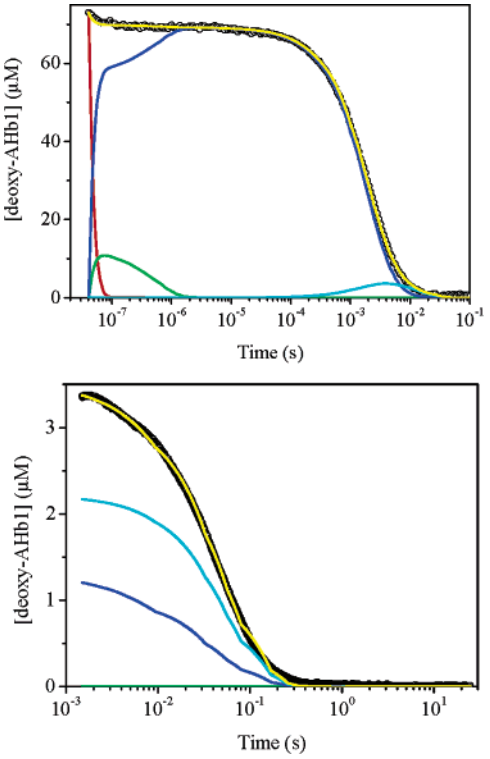

Figure 4. Results of global analysis of the CO binding kinetics to AHb1 from stopped flow (bottom panel, 0.05 atm CO) and laser flash photolysis (top panel, 0.3 atm CO) at $T = 25$ °C. The fits (yellow lines) are superimposed to the experimental data (circles). In the figure the time course of the other relevant species shown in Scheme 1 are reported: Hb_p:*CO* (red), Hb_p:*CO* (green), Hb_h (cyan), Hb_p (blue).

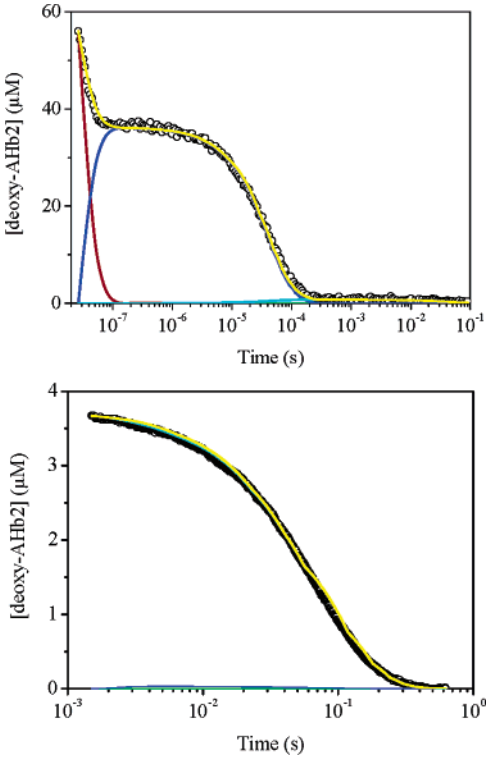

Figure 5. Results of global analysis of the CO binding kinetics to AHb2 from stopped flow (bottom panel, 0.05 atm CO) and laser flash photolysis (top panel, 0.7 atm CO) at $T = 25$ °C. The fits (yellow lines) are superimposed to the experimental data (circles). In the figure the time course of the other relevant species in Scheme 1 are also reported: Hb_p:*CO* (red), Hb_p::*CO* (green), Hb_h (cyan), Hb_p (blue).

attributed in Scheme 1 to the existence of a second internal docking site. The numerical analysis shows that the experimental curves are consistent with the existence of a route leading, with a high rate, to an internal docking site, from which the ligand quickly returns to the primary docking site and eventually exits to the solvent phase. This process is very weakly temperature dependent, suggesting that the access route to this secondary docking site is open and does not require movements of bulky side chains.

Figures 4 and 5 report the results of the kinetic analysis, under selected conditions (see corresponding figure captions for details), to CO binding kinetics in laser flash photolysis and stopped flow to AHb1 and AHb2. At each temperature, and for each protein, we were able to reproduce the CO binding kinetics with a single set of rate constants at all CO concentrations tested. The rate constants at 20 °C are reported in Table 1, along with the corresponding activation parameters.

The time course of the species in Figure 4, reporting the CO binding and rebinding kinetics to AHb1 for selected conditions, clearly highlights the effect of the equilibrium between the 6cLS and the 5cHS species in the stopped-flow data, where the relative contribution of each is clearly discernible. The geminate phase in the laser flash photolysis data can be reproduced using a model where the photolyzed CO can quickly migrate, with relatively low efficiency, to an internal docking site from which it escapes on longer time scales. The population of CO in this docking site is shown as a green line. Competition of the internal HE7 ligand for binding to heme is observed in the millisecond time range (cyan line). The 6cLS species, which is transiently formed, is then replaced by the carboxy species. Fitting of the stopped-flow trace in Figure 4 with a double exponential decay yielded lifetimes of 41 ms (35%) and 120 ms (65%). The fractions of fast and slow rebinding species are in agreement with the fractions of 5cHS (40%) and 6cLS (60%) species estimated from absorption spectra at equilibrium. With an equilibrium constant between 5cHS and 6cLS species of 1.6, a dissociation rate constant of about 10 s^{-1} (as estimated from the slow phase observed in stopped-flow experiments at high CO concentrations) results in an association rate constant on the order of 20 s^{-1}. This time scale is overlapping with the bimolecular rebinding kinetics, and omitting the equilibrium 5cHS $\rightleftharpoons$ 6cLS in the overall kinetic scheme fails to reproduce the rebinding kinetics.

The time course of the species for AHb2 is much simpler (shown in Figure 5 for selected conditions), with the stopped-flow data being dominated by replacement of the HE7 ligand by CO. No evidence for secondary docking of CO into an internal hydrophobic cavity was obtained from laser flash photolysis data, which suggested escape to the solvent with a strongly temperature-dependent process. The internal HE7 ligand competes in the 100-μs time range and is then very slowly replaced by CO within 1 second. The facile temporal separation of the two events (HisE7−Fe association vs dissociation) permitted them to be distinguished quite clearly in the laser flash photolysis signals.

The set of parameters determined at each temperature allowed for accurate reproduction of the kinetics measured in flash photolysis experiments as a function of CO concentration at that temperature. Very good fits were obtained with only minor adjustments of the rates and the CO concentration, thus

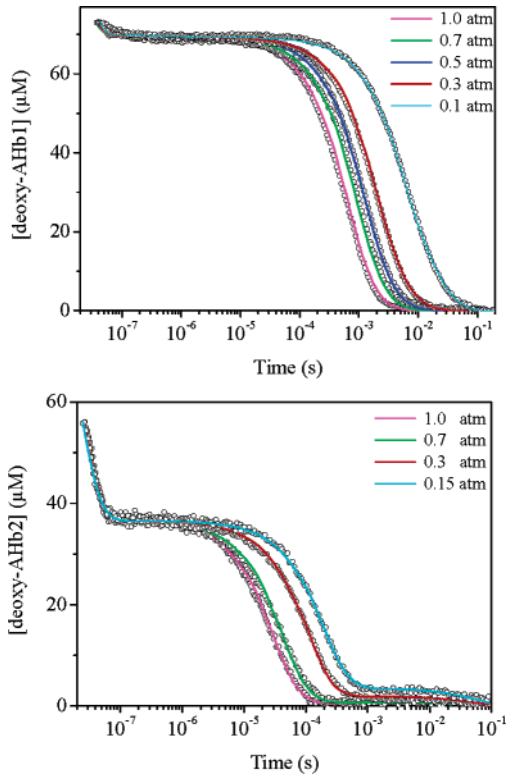

Figure 6. Results of global analysis of the CO rebinding kinetics to AHb1 (top) and AHb2 (bottom) after laser flash photolysis at several CO partial pressures at $T = 25$ °C. Open circles are the experimental data, and solid lines are the result of the best fit with Scheme 1. The color code for CO partial pressure is indicated in the caption. The rate constants used in the calculations were optimized starting from the values obtained in the global fits on stopped-flow and flash photolysis binding curves. The best fit was obtained with only minor adjustments of the rate constants. Similar analyses were performed on stopped-flow binding kinetics at different CO partial pressures and yielded consistently good fits (data not shown).

demonstrating the stability of the retrieved set of parameters. Examples are shown in Figure 6 for AHb1 and AHb2, respectively.

Table 1 reports the rate constants at 20 °C and the activation parameters retrieved from the fits to the experimental data using the reaction Scheme 1. Several of the parameters appearing in Scheme 1 (k_3, k_{-3}, k_a, and k_{-a}) play a minor role, with only marginal or no influence on the observed kinetics, and are consequently not reported in Table 1.

The difference in the extent of the geminate phase between the two proteins is largely due to the difference in the values of k_{-1}, which in both cases is a barrierless process within the investigated temperature range as observed for myoglobin,[47,67,69] human HbA,[16,62] and Ngb.[37,70] The rates k_{-1} are much higher than that recently reported for myoglobin in silica gels ($\sim 10^6$ s^{-1} [67]), and more similar to what was found for Hb gels bathed in aqueous buffer solutions ($\sim 5 \times 10^6$ s^{-1} [16,62]) or Hb gels in the presence of 80% glycerol ($\sim 20 \times 10^6$ s^{-1} [16,62]).

It is useful to estimate the bimolecular binding rate constant, usually termed k_{ON},[37,71] which is 1.22×10^6 M^{-1} s^{-1} for AHb1 and 2.99×10^7 M^{-1} s^{-1} for AHb2 at 20 °C. Previous determinations of k_{ON} for hemoglobins from *A. thaliana* have shown scattered values. For AHb1, Watts et al. measured values of $k_{ON} = 0.55 \times 10^6$ M^{-1} s^{-1} and for AHb2 $k_{ON} = 2.2 \times 10^7$ M^{-1} s^{-1}.[12] More recently, Uzan et al. reported a $k_{ON} = 5 \times 10^7$ M^{-1} s^{-1},[38] although it was unclear which of the three globin genes from *A. thaliana* was investigated. In general, our determinations agree with the values of k_{ON} observed for other hexacoordinated hemoglobins [e.g., human Ngb ($k_{ON} = 6.5 \times 10^7$ M^{-1} s^{-1},[72] $k_{ON} = 3.8 \times 10^7$ M^{-1} s^{-1} [65]), murine Ngb ($k_{ON} = 7.2 \times 10^7$ M^{-1} s^{-1},[72] 5.5×10^7 M^{-1} s^{-1} [37]), tomato SOLly GLB1 ($k_{ON} = 3.0 \times 10^7$ M^{-1} s^{-1} [23]), rice Hb1 ($k_{ON} = 6.8 \times 10^6$ M^{-1} s^{-1},[64] $k_{ON} = 6.8 \times 10^7$ $M^{-1}s^{-1}$ [23])].

The CO binding kinetics of AHb2 in stopped-flow experiments at high CO concentrations is entirely determined by the slow dissociation rate of the HisE7 ligand (k_{-b}).[37] This step is also responsible for the slower part of the biphasic kinetics measured for CO binding to AHb1, the faster being due to binding to the 5cHS fraction. The value of k_{-b}, which is identical in both proteins, is comparable to previous determinations (~ 40 s^{-1},[38] ~ 34 s^{-1} [39]). For human Ngb, His deligation rates are highly scattered, with reported values of 8200 s^{-1},[7] 4.5 s^{-1},[72] and 0.6 s^{-1}.[39] The available determinations of the k_{-b} for mouse Ngb were on the low side of the above range, with values of 1.2 s^{-1} [72] and 0.5 s^{-1}.[39] A recent study reported a value of 200 s^{-1} for the k_{-b} of tomato SOLly GLB1.[23] Interestingly, in the case of tomato SOLly GLB1, k_b is identical to k_{-b}, thus leading to an equilibrium between 5cHS and 6cLS species for the deoxy Fe^{2+} state,[23] very similar to the case of AHb1, for which the rates k_{-b} and k_b are comparable. On the contrary, the 6cLS is favored in Fe^{2+}AHb2 since $k_b \approx 30 \times k_{-b}$. However, the relatively small value of k_b allows binding of the endogenous ligand with small efficiency on the time scale of the flash photolysis experiment (Figure 3).

Incidentally, we noted that the much higher values of k_{ON} and k_b for AHb2, as compared to the corresponding parameters in AHb1, explain why the slow phase associated with HisE7 replacement by CO is much more discernible in the rebinding kinetics to AHb2 (Figure 3). The ligand binding in solution (rate k_{-2}) has very similar activation enthalpies and entropies for both proteins (Table 1), suggesting that the viscosity of the solution determines the barrier.[37] On the other hand, the barriers for the exit to the solvent (rate k_2) do not share the same similarity, being higher in the case of AHb2. The His ligation step (k_b) is characterized by a lower enthalpic barrier in AHb2 than in AHb1, in agreement with the more favorable binding of the endogenous ligand. In contrast, the entropic terms are identical. The enthalpic and the entropic barriers for k_{-b} are the same in both proteins. The only previous determination for an Hb from *A. thaliana* reported a value of 22.5 kcal/mol, only slightly higher than our previous estimate.[38] It is worthwhile noticing that the barriers for AHb1 and AHb2 are comparable with, although a bit smaller than, the value for the dissociation of the endogenous His ligand in murine Ngb ($\Delta H^{\ddagger} = 25 \pm 1$ kcal/mol[37]) and human Ngb (24 kcal/mol[38]).

Two important questions remain, namely the source of the remarkably different reactivity of the two Hbs and why the extent and the temperature dependence of the geminate phases are so different. The dramatic difference in the amplitude of

(69) Agmon, N. *Int. J. Chem. Kinet.* **1981**, *13*, 333−365.
(70) Nienhaus, K.; Kriegl, J. M.; Nienhaus, G. U. *J. Biol. Chem.* **2004**, *279*, 22944−22952.
(71) Henry, E. R.; Sommer, J. H.; Hofrichter, J.; Eaton, W. A. *J. Mol. Biol.* **1983**, *166*, 443−451.
(72) Dewilde, S.; Kiger, L.; Burmester, T.; Hankeln, T.; Baudin-Creuza, V.; Aerts, T.; Marden, M. C.; Caubergs, R.; Moens, L. *J. Biol. Chem.* **2001**, *276*, 38949−38955.

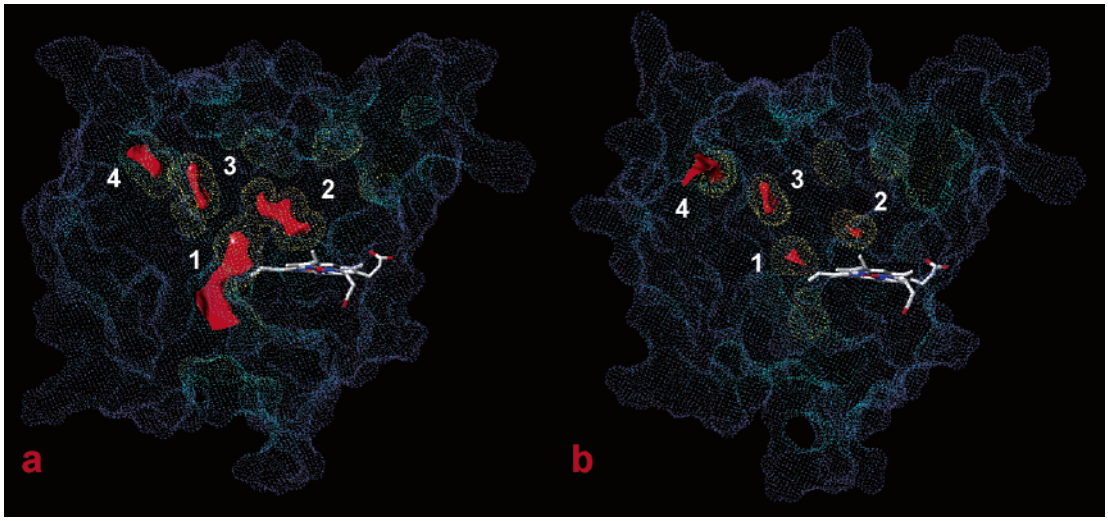

Figure 7. Comparison between the Connolly surface profiles and the cavity locations identified in AHb1 (a) and AHb2 (b). Dotted surfaces are built with Sybyl MOLCAD tools as a depth function. External protruding regions are colored blue, while cavities and clefts are progressively colored green, yellow, and orange. The red-colored contours correspond to the energetically and sterically favorable regions for Xe/hydrophobic binding, identified by the software GRID. All the cavities not highlighted by the green GRID contours are isolated and/or directly connected to the bulk.

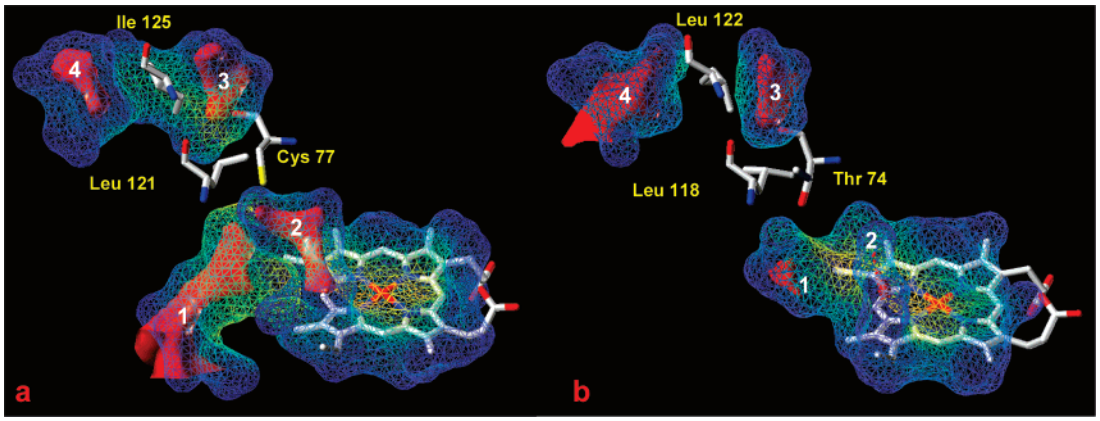

Figure 8. Close-up view of the internal cavities network of AHb1 (a) and AHb2 (b). The heme group and the critical residues, regulating the communication between the different cavities, are displayed in capped sticks. The red-colored contours correspond to the energetically and sterically favorable regions for Xe/hydrophobic binding, identified by the software GRID.

the geminate phase calls for a substantial difference in ligand migration pathways inside the protein and, through the protein matrix, to the solvent phase. In the absence of crystallographic structural data we have built structures for both AHb1 and AHb2 by homology modeling[15] and have located interior hydrophobic cavities which may modulate ligand dynamics (Figure 7). Hydrophobic cavities for both AHb1 and AHb2 were localized by exploring the protein matrix using the software GRID[20] and a Xe atom as a probe, a search procedure that, recently applied to myoglobin,[16] correctly identified the crystallographically detected Xe1, Xe3, and Xe4 sites.[51]

A simple visual inspection of the Connolly surface maps built for AHb1 and AHb2 evidences significant difference in the extension and the volume of the internal cavities, further confirmed by the calculation of the corresponding area and volume values (Table 2), performed with the program Grasp.[19] The most striking difference is represented by the deep hydrophobic channel (cavity **1** in Figures 7a and 8a), which is present only in AHb1, connecting the heme binding pocket with the solvent through the distal cavity (cavity **2** in Figures 7a and 8a). A deep and profound cleft (cavity **4**) is located on the protein surface and is accessible to cavity **3** (and thus to cavity **2)** through the movements of a few amino acids (Figure 8a).

Table 2. Surface and Volume of the Cavities, Detected by PASS,[17] Calculated Using Grasp[19]

cavity #	1	2	3	4	total
		AHb1			
area (Å^2)	212	145	109	166	632
volume (Å^3)	150	83	67	113	412
		AHb2			
area (Å^2)	60	67	71	140	338
volume (Å^3)	33	33	43	96	205

The heme binding pocket (cavity **2**) of AHb2 (Figure 7b) is not directly accessible from the solvent, since the channel present in AHb1 is obstructed by the methyl-propyl side chain of Leu147. The corresponding residue in AHb1 is Ala150, whose smaller methyl side chain allows communication with the exterior. The volume of cavity **1** is significantly reduced in comparison with the corresponding cavity in AHb1. The presence of Phe32 and Val114 side chains in AHb2, substituting Leu35 and Ala117 in AHb1, interrupts the communication between cavities **1** and **2**. The reduced dimensions of cavities **2** and **3** are expected to make the migration more difficult (Figure 8b). On one side, cavity **4** in AHb2 is directly connected with

the solvent, as in AHb1, while on the other side it is connected with cavity **3** through movement of the side chain of Leu122 (Figure 8b).

It is worthwhile noticing that the cavity pattern of the homologous rice hemoglobin, whose three-dimensional structure was used to model the structures of AHb1 and AHb2, is extremely different, showing only a small cleft placed over the heme group, with a volume of just 24 $Å^3$. The total volume of the cavities in AHb1 is slightly larger than the overall volume of the apolar tunnels in *Chlamydomonas eugametos* (320 $Å^3$) and *Mycobacterium tuberculosis* (330 $Å^3$) truncated Hb,[73,74] and about 2-fold larger than the volume of the cavities in *Paramecium caudatum* truncated Hb (180 $Å^3$).[73] However, quantitative comparison is difficult since different programs and different conditions were used to identify the cavities and calculate their corresponding volumes.

On the whole, the structure of AHb1 seems to allow the rapid migration of ligands (e.g., CO) from the heme pocket to other potential binding sites or to the exterior, while in AHb2 ligands could be trapped in the accessible cavities for longer times. The lack of geminate rebinding and the small temperature dependence of the geminate phase in AHb1 seem to be consistent with the presence of a large hydrophobic tunnel connecting the distal cavity of AHb1 with the solvent. Small geminate phases at room temperature were also reported for truncated Hbs and for neuroglobin solutions.[37,38,75] The apolar tunnel in AHb1 closely resembles those reported for truncated Hbs[61,73−76] and for neuroglobin,[77−80] although the cavities extend from the distal cavity to the solution through different regions of the proteins. Despite the high reliability of the method, caution must be exercised concerning the detailed location and shape of the internal cavities, as they have been inferred from structures determined by homology modeling with respect to Fe^{3+} rice Hb. The CO ligated structures may differ from the above, due to structural rearrangements following ligation, as has been shown recently for neuroglobin.[78] A definitive description of the cavities will be possible only after the three-dimensional structures become available.

The apolar interior of the tunnel can increase the solubility of nonpolar diatomic molecules such as CO relative to the aqueous phase, thus enhancing the local effective concentration of heme ligands.[61] The observed kinetic properties and the structural features argue in favor of a putative NO-dioxygenase role played by AHb1 in counteracting nitrosative stress,[11] as previously proposed for *M. tuberculosis* truncated Hb.[73,76] In the truncated Hbs from *M. tuberculosis*, *P. caudatum*, and *C. eugametos* the NO conversion to NO_3^- at the heme distal site may be promoted not only by a hydrogen-bonding network polarizing the iron-coordinated O_2 molecule but also by the easy diffusion of the molecular partners (i.e., O_2 and NO) from the solution to the distal heme cavity, the accumulation of reactants along the hydrophobic tunnel path, and the fast and efficient removal of the polar product (NO_3^-) out of the reaction cavity to the solvent space.[73] Recent extended molecular dynamics simulations on *M. tuberculosis* truncated Hb suggest that trHbN has evolved a dual-path mechanism for migration of O_2 and NO to the heme in order to achieve the most efficient NO detoxification.[81]

In summary, AHb1 and AHb2 show remarkably different interactions of the distal cavity residues with both the heme and ligands. The dramatic differences in reactivity with exogenous ligands appear to be related with a very different system of hydrophobic cavities. These properties argue in favor of distinct functions for the two globins and for AHb1 suggest a possible mechanism similar to that hypothesized for the NO-dioxygenase activity of neuroglobin and truncated hemoglobins.

Acknowledgment. The authors acknowledge MIUR (PRIN-2004) for financial support.

JA066638D

(73) Milani, M.; Pesce, A.; Ouellet, Y.; Dewilde, S.; Friedman, J.; Ascenzi, P.; Guertin, M.; Bolognesi, M. *J. Biol. Chem.* **2004**, *279*, 21520−21525.
(74) Milani, M.; Pesce, A.; Ouellet, Y.; Ascenzi, P.; Guertin, M.; Bolognesi, M. *EMBO J.* **2001**, *20*, 3902−3909.
(75) Giangiacomo, L.; Ilari, A.; Boffi, A.; Morea, V.; Chiancone, E. *J. Biol. Chem.* **2005**, *280*, 9192−9202.
(76) Pesce, A.; Couture, M.; Dewilde, S.; Guertin, M.; Yamauchi, K.; Ascenzi, P.; Moens, L.; Bolognesi, M. *EMBO J.* **2001**, *19*, 2424−2434.
(77) Pesce, A.; Dewilde, S.; Nardini, M.; Moens, L.; Ascenzi, P.; Hankeln, T.; Bolognesi, T. B. *Structure* **2003**, *11*, 1087−1095.
(78) Vallone, B.; Nienhaus, K.; Matthes, A.; Brunori, M.; Nienhaus, G. U. *Proc. Natl. Acad. Sci. U.S.A.* **2004**, *101*, 17351−17356.
(79) Vallone, B.; Nienhaus, K.; Matthes, K.; Brunori, M.; Nienhaus, G. U. *Proteins* **2004**, *56*, 85.
(80) Brunori, M.; Gibson, Q. H. *EMBO Rep.* **2001**, *2*, 674−679.
(81) Bidon-Chanal, A.; Martí, M. A.; Crespo, A.; Milani, M.; Orozco, M.; Bolognesi, M.; Luque, F. J.; Estrin, D. A. *Proteins* **2006**, *64*, 457−464.